Materials Innovations

HΣXA Publishers

Carbon Materials | Research Article | http://doi.org/10.54738/MI.2022.2804

Role of Hydrogen Flow Rate for the Growth of Quality Nanodiamonds via Microplasma Technique

Saman Iqbal[1], Muhammad Shahid Rafique[2], Sultan Akhtar[3], Nida Iqbal[4], Faryal Idrees[1]*, Arshad Mahmood[5]

1 Department of Physics, University of the Punjab, Lahore, Pakistan
2 Department of Physics, University of Engineering and Technology, Lahore, Pakistan
3 Department of Biophysics, Institute for Research and Medical Consultations, Imam Abdulrahman bin Faisal University, Dammam, Saudi Arabia
4 Biomedical Engineering Centre, University of Engineering and Technology, Kala Shah Kaku (KSK) Campus, Lahore
5 National Institute of Lasers and Optronics (NILOP), P.O. Nilore, Islamabad, Pakistan

OPEN ACCESS

Article is part of Special issue on "WEmpower Pakistan in Materials Science Research for SDGs"

Received: 10 May 2022

Accepted: 16 July 2022

Published: 28 August 2022

Editor(s): Hassina Tabassum

Citation: Iqbal S, Shahid Rafique M, Akhtar S, Iqbal N, Idrees F, Mahmood A (**2022**) Role of Hydrogen Flow Rate for the Growth of Quality Nanodiamonds via Microplasma Technique. *Materials Innovations 2* (8), 214-224.

***Correspondence**: (Faryal Idrees) faryal.physics@pu.edu.pk

Published By Hexa Publishers

ISSN
Electronic: 2790-1963

Nanodiamonds (NDs) were prepared by utilizing a microplasma facility. Ethanol and Argon mixture was decomposed in microplasma for the formation of NDs. In order to stabilize the NDs growth, the Hydrogen was added in the mixture during the growth process. Hydrogen flow rate was changed from 1 to 5 L/min to find out the optimum flow rate for the growth of stabilized NDs. The experiments were also performed without the introduction of Hydrogen for the comparison. TEM and Raman analysis confirm that the highest quality diamonds are obtained at Hydrogen flow rate of 3L/min. In the case of Hydrogen, the SAED patterns reveal the presence of pure diamond phases which in turn envisages the etching of graphitic shell. TEM micrographs reveal that the size of NDs produced at 3 L/min Hydrogen flow rate ranges from 1~20 nm which is much smaller than that of without Hydrogen (4-32 nm). EDX spectra also disclose the Carbon peak with a maximum intensity for 3 L/min flow rate. UV-Visible and PL spectroscopy analysis indicate the presence of Nitrogen-Hydrogen defect centers. However, a decrease in defect density at 3L/min indicates the production of improved quality NDs. FTIR also verifies the removal of graphitic shell around NDs at 3 L/min flow rate. Moreover, high hydrogen flow rates effectively incorporate nitrogen vacancy (NV) defects. Prepared NDs offer emerging applications in optoelectronic systems, biomedical nanodevices and nanoscale sensors for electric field, magnetic field & temperature

Keywords: Microplasma, Quenching, Nanodiamonds, SAED, Nitrogen Vacancy (NV) Defects

INTRODUCTION

Nanodiamonds (NDs) have received considerable attention across the world in the past decades. NDs offer potential applications in electronics, spintronics, electrochemistry, miniaturized mechanical and optoelectronic systems, seed during chemical vapor deposition (CVD) of diamond films, biomedical nanodevices, humidity

resistant membrane, etc. NDs can be synthesized by using various methods such as detonation, pulsed laser ablation, CVD etc[6,7]. But the issues related to NDs properties (structural, morphological, surface) and overall cost (production rate, safety) of the processing are still under consideration[8].

Atmospheric pressure microplasma (AMP) or microplasma is a new class of plasmas. Microplasma is stabilized by a large concentration of energetic electrons (1-10 eV) at high pressure while maintaining relatively low gas temperature. The current and energy densities in plasma are found to be high enough to maintain the extreme conditions required for NDs production[9–12]. The structure and phase state of NDs are effectively controlled by microplasma parameters such as gas flow rate, composition, pressure and voltage, etc.[2,12–15]

Gas flow is a valuable parameter to maintain the non-equilibrium condition of microplasma[2,15]. Gas phase synthesis of nanoparticles requires decomposition of vapor precursors by electron impact dissociation in microplasma. This process creates radical moieties which can nucleate particles. High gas flow rates restrict the excessive particle growth in the reactor[9].

The role of hydrogen can't be ignored in production of high good quality NDs[14]. The desorption and diffusion of Hydrogen tune phase transitions. Atomic Hydrogen dissociates methane (CH_4) into methyl radical CH_3 which plays critical role in diamond growth[14,16]. The saturation of dangling bonds prevents the graphitization of diamond surfa. The etching rate of hydrogen to sp^2 Carbon (Graphite) is much faster than sp^3 Carbon (diamond)[12,14,16]. Finally, rapid decomposition of larger hydrocarbon fragments via atomic hydrogen prevents polymers or ring structure formation[14,16].

In this project, we have employed a micro plasma facility for the fabrication of NDs. The purpose is to explore the role of Hydrogen flow rate on structural, optical, and surface properties of NDs.

EXPERIMENTAL SETUP

The self-designed microplasma chamber was used to perform experiment. The details are described in[2,14]. Flow setup has been used to control the flow of precursor (Ethanol), carrier gas (Argon), and quenching/stabilizing agent (Hydrogen) via mass flow controllers (MFC) and exhausts. Hydrogen was introduced indirectly in argon and ethanol mixture. The details of indirect hydrogen dilution flow setup is described in[14]. Flow rate of Argon was kept constant at 5 L/min, and flow rate of Hydrogen was varied from 1-5 L/min. The microplasma dissociated the mixture of Argon and Hydrogen gas with Ethanol vapors in chamber at atmospheric pressure. The discharge was obtained at a constant current of 2 mA and voltage of 2.5 kV. This process continued for 10 minutes. The synthesized NDs were collected in acetone. NDs were characterized by various characterization techniques.

RESULTS AND DISCUSSION

TEM analysis

Figure 1 represents the TEM analyses of NDs (a-b) selected area electron diffraction (SAED patterns, (c-d) TEM images and (e-f) EDX in case without and with Hydrogen at a flow rate of 3 L/min. This specimen was chosen because the highest diamond contents (extracted from Raman analyses) were obtained at this flow rate. For the sake of comparison, a specimen of NDs without Hydrogen was Figure 1 shows SAED patterns of NDs without (a) and with Hydrogen at 3 L/min (b). Figure 1 (a) reflects two bright rings associated with (110) and (100) planes of diamond reference. The d-spacing of NDs correlates with the lonsdaleite diamond (JCPDS-19-268)[14]. The lonsdaleite is often found in meteorites[12,17].

There is also the presence of graphitic shell (002) plane as confirmed from d-spacing (JCPDS-65-6212)[18]. The lattice d-spacing of three rings calculated from SEAD data is given in table 1.

Microplasma produces high-density non-equilibrium plasma within time intervals ~ millisecond. During nucleation, precursors are introduced into the microplasma. Electron impact dissociation of precursor resulted in reactive radical species (C_2H^+, $C\ H_3$) and simultaneous formation of sp^3 and sp^2 Carbons[14]. The buckling of the basal planes of Graphite as a diffusion less process results in lonsdaleite diamond formation[14,19]. It is considered as an intermediate state of transforming Graphite into diamond[20]. Lonsdaleite and graphite have same orientation relation. Thus, less coherent energy is required at Graphite/lonsdaleite interface. This makes lonsdaleite diamond formation kinetically favorable over cubic diamond[21].

Figure 1b exhibits that the introduction of Hydrogen produces (100) and (102) planes of lonsdaleite diamond. The appearance of new (002) plane is associated with n-diamond (metastable Carbon polymorph). it is occasionally occurred along with lonsdaleite diamonds[14,17].

Another way to produce diamond is diffusion-controlled nucleation and successive crystal growth process. Lattice defects and crystal surfaces with dominant sp^3 hybridized dangling bounds are origin of this process[14,19]. Enough supply of Hydrogen is efficiently incorporated to lead the diffusion mechanism. The saturation of dangling bonds via Hydrogen prevents graphitization of diamond surface[14,16]. It etches sp^2 Carbon much faster than sp^3 Carbon[14]. Thus, hydrogen promotes diamond growth and suppresses non-diamond phases. The absence of graphitic shell in NDs (Figure 1b) is taken as evidence.

Figure 1 represents the TEM images of NDs in case without Hydrogen (Fig-

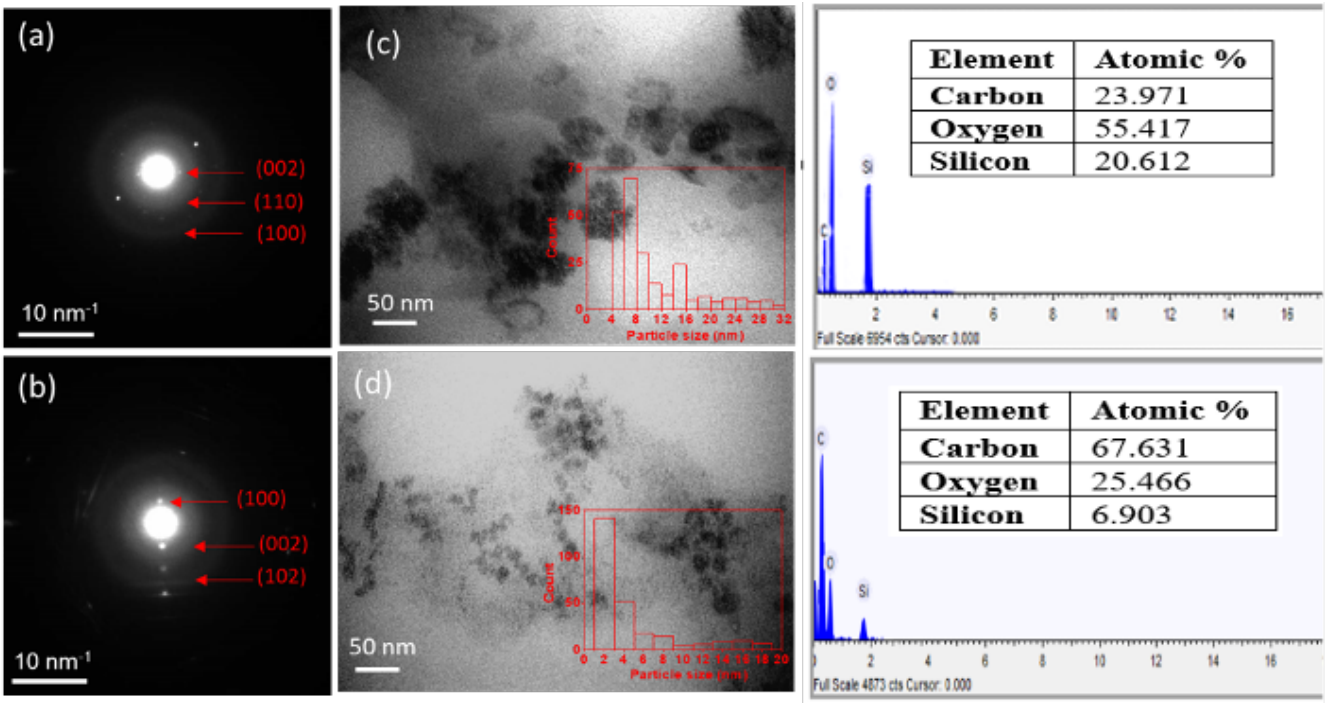

Figure 1. TEM images of NDs (a) without Hydrogen and (b) with Hydrogen at flow rate of 3 L/min along with corresponding SAED patterns (c, d) and EDX (e, f). Inset is histogram of NDs representing particle size distribution. The main reflections of NDs are indexed in the pattern.

*Table 1. d-spacing measured from SEAD pattern (Where, G= graphite, L= lonsdaleite diamond and *C= forbidden cubic diamond)*

Sample	Calculated d-spacing (nm)	Experimental d-spacing (nm)	hkl
Without Hydrogen	0.330	0.335	$(002)^{G}$
	0.250	0.252	$(110)^{L}$
	0.212	0.218	$(100)^{L}$
	0.217	0.218	$(100)^{L}$
With Hydrogen at 3L/min	0.181	0.178	$(002)^{*C}$
	0.148	0.150	$(102)^{L}$

ure 1 c), and with Hydrogen at 3 L/min (Figure 1 d). It was observed that NDs have nearly spherical geometry in both the cases. A reduction in particle size is observed because with the introduction of Hydrogen, the non-diamond phases are etched away, and only crystalline phases remain. It is confirmed by particle size histogram inset in Figure 1 (c-d). The particle size of NDs was evaluated by using Image J software. NDs are synthesized in four steps. Initially, hydrocarbons-Hydrogen gas mixture is dissociated. The simultaneous formation of sp^3 and sp^2 Carbons occur in second step. Diamond as kinetically stable state of Carbon requires rapid cooling. Hydrogen quenches the dissociated gas mixture to preserve sp^3 Carbon. Hydrogen also etches the sp^2 Carbons (non-diamond form) [14] . Thus, smaller and crystallized NDs are obtained upon using Hydrogen compared to growth of NDs without Hydrogen.

Figure 1 shows the EDX spectra of NDs without (Figure 1 e) and with Hydrogen at flow rate 3 L/min (Figure 1 f). EDX spectra confirm the purity of synthesized NDs. It contains only three elemental peaks of Carbon, Oxygen and Silicon. Carbon peak is related to the formation of diamond and non-diamond contents. Silicon peak appears due to the substrate. Oxygen peak might originate from the environment or due to the substrate.

Raman spectroscopy

Figure 2 (a) shows Raman spectra (after base subtraction) obtained from NDs produced without and with Hydrogen at different flow rates. All the spectra show broad bands located around 1081-1142 cm^{-1}(t-PA-band),1301-1329 cm^{-1}(Dia-band), 1355-1412 cm^{-1}(D-band) and 1571-1587 cm^{-1}(G-band).

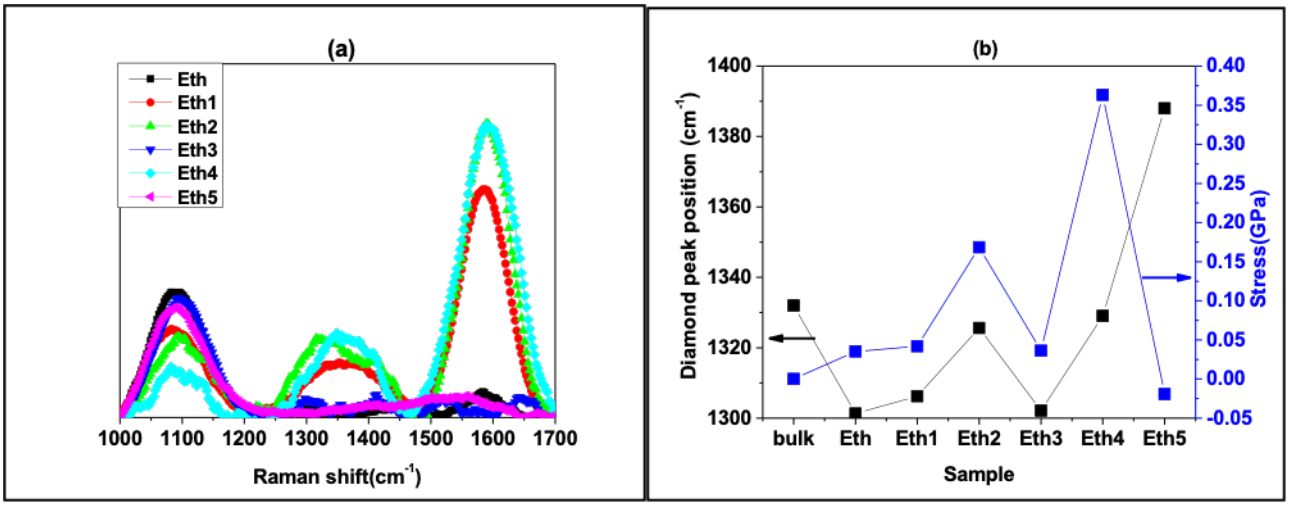

Figure 2. (a) Raman spectra of NDs without and with different Hydrogen flow rates, (b) variation of diamond peak position and stress at different Hydrogen flow rates. where Eth= constant Argon flow rate= 5 L/min, Ethi= Hydrogen flow rate, i= 1-5 L/min.

Deconvolution and Gaussian peak fitting of Raman spectrum of NDs at Hydrogen at 3 L/min is presented in supporting material Figure S1. This particular flow rate has been selected because at this flow rate maximum intensity of diamond band is obtained.

Raman line (1081-1142 cm^{-1}) is considered as direct evidence of nanocrystalline diamond (NCD)[2,14] . Ferrari and Robertson, related the observed bands at 1080-1150 cm^{-1} and 1426-1472 $cm^{-1}$with Trans- polyacetylene (t-PA) at the surface and grain boundaries of NCD[22] . The degree of inhomogeneity of trans-CHx chains strongly affect the position, shape and intensities of trans-CHx modes.[2,14]

Ethanol conversion proceeds through two main reactions,

$C_2H_5OH \rightarrow 2.5\ H_2+CO+0.5\ C_2H_2$ (1)

$C_2H_5OH \rightarrow H_2+CO+\ CH_4$ (2)

Conversion of Ethanol into acetylene (reaction 1) is the main process throughout the Hydrogen flow range. The dominance of Ethanol conversion to methane over acetylene (reaction 2) results in decreasing trend of t-PA with increasing Hydrogen flow rate. However, the D and G band intensities are found to be increasing with the increase in the flow rate of Hydrogen.

The Raman peak of bulk diamond is found at 1332 cm-1[12] . The observed Raman peak position of NDs without Hydrogen is found at 1301 cm^{-1} and the ones with Hydrogen at different flow rates are found at, 1306 cm^{-1}(1 L/min), 1325 cm^{-1} (2 L/min), 1302 cm^{-1}(3 L/min) and 1329 cm^{-1}(4 L/min). The Raman peak appearing in the range of 1301-1329 cm^{-1} at different Hydrogen flow rates are associated with crystalline diamond and is known as diamond band. The phonon confinement effect is the main reason behind this downshifting of the Raman peak with respect to bulk diamond[1,23,24] and decrease in grain size. The smallest grain size is obtained at a flow rate of 3 L/min.

Figure 2(b) shows a corelation between stress and diamond peak position at different Hydrogen flow rates. The degree of stress was estimated using the formula in[25] . For Hydrogen flow rate (0-1 L/min), the higher value of tensile stresses (see supporting material (table 2)) generated from vacancies, dislocation and grain boundary[26] red shift diamond peak position as compared to bulk (1332 to 1301 cm^{-1}). The decrease in tensile stresses with the increment in Hydrogen flow rate (1-4 L/min) shift the peak to relatively higher wave number (from 1301 to1329 cm^{-1}). The dominance of non -diamond phases on the highest Hydrogen flow rate (5 L/min) creates compressive stresses. These stresses are responsible for further shift the peak from 1329-1388 cm^{-1}. Thus, at highest flow rate, we got the lowest diamond quality (as compared to other flow rates), higher disordered structure[26] . D (disorder)-band (1355-1413 cm^{-1}) is a combination of highly defective sp^3 Carbon (diamond-like Carbon (DLC)) and disordered sp^2 Carbon (graphitic D-band)[2,14] . G-band (1573-1587cm^{-1}), structural nanographite is related to zone-center phonon scattering of E_{2g} symmetry of sp^2Carbon materials[12] . With the increase in Hydrogen flow rate from (0-5 L/min), G-band is shifted towards lower wave number until the lowest value from 1587 to 1571 cm^{-1}, respectively. The structural defects as origin of stresses shift the G-band. These stresses (see supporting material (table S1)) change the bond length. The G-band shifting towards higher wavenumber is related to shorter bond length or vice versa.

Table 2. Raman spectroscopy data of NDs without and with different Hydrogen flow rates

Sample	Peak position (cm^{-1})	Raman bands	FWHM (cm^{-1})	I_{Dia}/I_G	L_{Dia} (nm)	$I_{D/G}$	L_D (nm)	Amount of Diamond (%)	sp^3 content	Stress (diamond) (Gpa)
Eth (Ar=5L/min)	1092.58	t-PA (v_1 mode)	97.21	0.299	14.61	0	0	90.79	0.210	0.035
	1301.33	Dia-band	44.25							
	1456.79	t-PA (v_3 mode)	83.35							
	1586.10	G-band	67.27							
Eth1 (Ar=5L/min+ H=1L/min)	1089.71	t-PA (v_1 mode)	51.97	0.118	36.86	0.188	23.21	86.821	0.216	0.042
	1306.21	Dia-band	15.69							
	1368	D-band	24.92							
	1426.45	t-PA (v_3 mode)	11.32							
	1584.92	G-band	132.17							
Eth2 (Ar=5L/min+ H=2L/min)	1096.72	t-PA (v_1 mode)	47.37	0.287	15.23	0.142	30.94	94.81	0.215	0.168
	1325.58	Dia-band	48.91							
	1413.79	D-band	24.08							
	1584.97	G-band	170.16							
Eth3 (Ar=5L/min+ H=3L/min)	1081.66	t-PA (v_1 mode)	46.91	2.67	1.64	2.61	1.67	99.63	0.241	0.036
	1126.95	t-PA (v_2 mode)	35.28							
	1302.14	Dia-band	10.61							
	1355.16	D-band	5.31							
	1411.13	D-band	10.36							
	1472.23	t-PA (v_3 mode)	5.04							
	1522.46	A-band	11.04							
	1579.76	G-band	3.97							
	1616.45	D'-band	5.05							
	1648.69	OH-group	12.04							
Eth 4 (Ar=5L/min+ H=4L/min)	1089.74	t-PA (v_1 mode)	31.14	0.217	20.08	0.171	25.71	91.34	0.205	0.363
	1329.02	Dia-band	37.11							
	1387.34	D-band	29.04							
	1587.01	G-band	170.27							
Eth5 (Ar=5L/min+ H=5 L/min)	1084.28	t-PA (v_1 mode)	86.87	0	0	0.812	5.38	0	0.282	0
	1142.48	Dia-band	89.61							
	1388.12	D-band	97.56							
	1504.06	A-band	112.31							
	1571.35	G-band	84.76							

Figure 3 (a) shows a graph between I_{Dia}/I_G and amount of diamond at varying Hydrogen flow rate. Both display similar trend. With the increase in the Hydrogen flow rate (0-2 L/min), a decrease in the I_{Dia}/ I_G ratio or amount of diamond is obseved. At this point, Hydrogen flow is too low or Argon dilution is too high for the production of diamond. The I_{Dia}/ I_G ratio or amount of diamond starts increasing until obtained the highest value at the optimal Hydrogen flow rate of 3 L/min due to etching effect of Hydrogen []. This flow rate 3L/min appears to be the optimum flow rate for the production of high quality NDs due to the highest diamond contents. Further increase in the Hydrogen flow rate (4-5L/min) reduces the value of I_{Dia}/I_G or amount of diamond. In other words, higher Hydrogen flow rate decreases Ethanol residence time in reactor. Higher velocity profile pushes off the Ethanol at a faster rate from the reaction zone. Thereby, suppressing the formation of diamonds[2,14] .

Figure 3 (b) shows varation of and I_D/I_G and sp^3 content with Hydrogen flow rate. Both follow the amorphization trajectory. The transformation of graphite to nanocrystalline graphite (0-3 L/min), nanocrystalline graphite to low sp^3 content (3-4 L/min) and finally conversion to highly sp^3content occurs at 5L/min. The suppression of diamond at high Hydrogen flow rates as discussed earlier enhances the chances of non-diamond growth (such as DLC). The transformation of trigonal bonds into tetrahedral bond results in an enhancement in bond angle disorder[27] . Thus, DLC instead of diamond is obtained as depicted by increasing trend of sp^3 content as well I_D/I_G ratio.

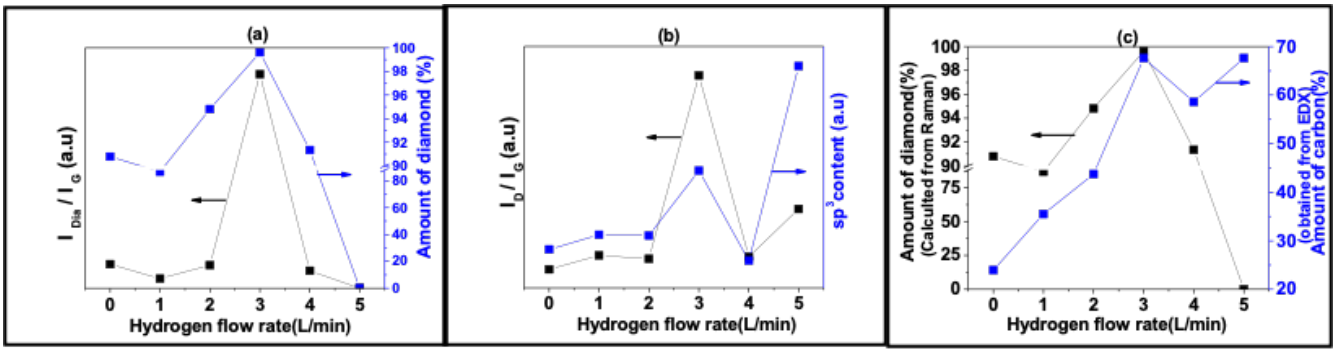

Figure 3. Variation of (a) I_{Dia} /I_G and I_D/I_G, (b) amount of diamond and sp^3 content without Hydrogen and with different Hydrogen flow rates: 1-5 L/min (c) Variation of calculated amount of diamond (calculated from Raman spectra and amount of Carbon (obtained from EDX) present within NDs at different Hydrogenn low rates.

The detail of Raman bands is given in supporting material (table S1)).

Figure 3 (c) shows a graph between the amount of Carbon (obtained from EDX) and amount of diamond (calculated from Raman) at different Hydrogen flow rates. Hydrogen quenched the diamond phases and etched the non-diamond phases of carbon inside the plasma volume. Finally, it comes out of the reactor volume. Thus, the resident time (flow rate) is important parameter to control this steady state process[13] . The relative amount of Carbon increases with diamond, confirming that most of the Carbon detected in EDX is in diamond form at 3 L/min. Thus, EDX supports Raman results. The flow rates higher or lower than the optimal value makes Hydrogen less efficient resulting into non-diamond Carbon.

UV-Vis Spectroscopy

Figure 4 (a) shows UV Visible spectra of NDs at different Hydrogen flow rates. All the spectra show an absorption peak at 390 nm with a peak around 363 nm and extended tail in the red region (600 nm). An additional peak at 536 nm is an interesting feature which has appeared at an optimal flow rate of 3 L/min. This peak is present for higher Hydrogen flow rate (4-5 L/min) as well. Broad absorption bands around 360, 390, 520-550 nm can be observed in type I, IIa synthetic diamond grown in Nitrogen environment[2,14,28] .

Far UV to visible absorption of diamond is result of Nitrogen, vacancy, and Hydrogen. NV is formed when an isolated Nitrogen atom is trapped by adjacent Carbon vacancy oriented along <111> in diamond lattice [,]. The negatively charged vacancy defect (NVH^-) is responsible for 393 nm and NV^0 defect is ascribed to 536 nm absorption in diamond[29] . The concentrations of NVH^- is higher than the NV centers. The intensities of UV-Visible absorption bands follow the order 393 nm (NVH) > 550 nm (possibly NV related) as previously reported in literature[30] .

Diamond is expected to be transparent in far UV to visible rang due to large band gap (~5.5 eV). However, any absorption in this region is result of defect formation during the growth process. Diamond growth takes place layer by layer on the nuclei. Slight disturbances in diamond formation creates spaces in planes for fluorescent optical defects[2,14] . The pinkish brown color emerges due to vacancy disks in{111} plane[24]. This coloration covers over whole visible spectral range with two additional bands (550 and 380 nm)[28]. Nitrogen is always found as a residual impurity in the chamber. Diamond fabricated at higher Hydrogen flow rate contains defects such as vacancy clusters. Nitrogen and Hydrogen incorporated them as NVH^-. At low flow rate (0-2 L/min) absorption is dominated only by these defects. As the optimal flow rate is attained (3 L/min), there is a reduction in absorption related to NVH followed by the introduction of NV is observed. The lower energy (~ 1 eV) formation of NVH complex makes them a competitive candidate of NV defect in diamond growth. The formation of stable C-H bonds on {111} plane of NDs phases enhances the mobility of Hydrogen[2,14] . Thus, the decrease in NVH defect correspondingly increases the NV. At higher flow rate (4-5 L/min), UV-Vis curves are signified by exponentially decay tail. The higher concentration of defects or unsaturated bonds is responsible for the existence of localized states in amorphous region[2,14] . Thus, high absorption in far UV to Visible is observed.

Various properties of NDs such as size, size distribution, shape, lattice parameters effect wavelength, position, and FWHM of surface plasmon resonance bands. The increase in number of peaks confirms the asymmetry in nanoparticles[31] . With the introduction of Hydrogen regardless of the flow rate, the peak is asymmetrically broadened towards higher wavelength. A stable position of absorbing peak at 393 nm indicates that particles do not aggregate[32] .

Figure 4 (b) shows a variation of the optical band gap and amount of

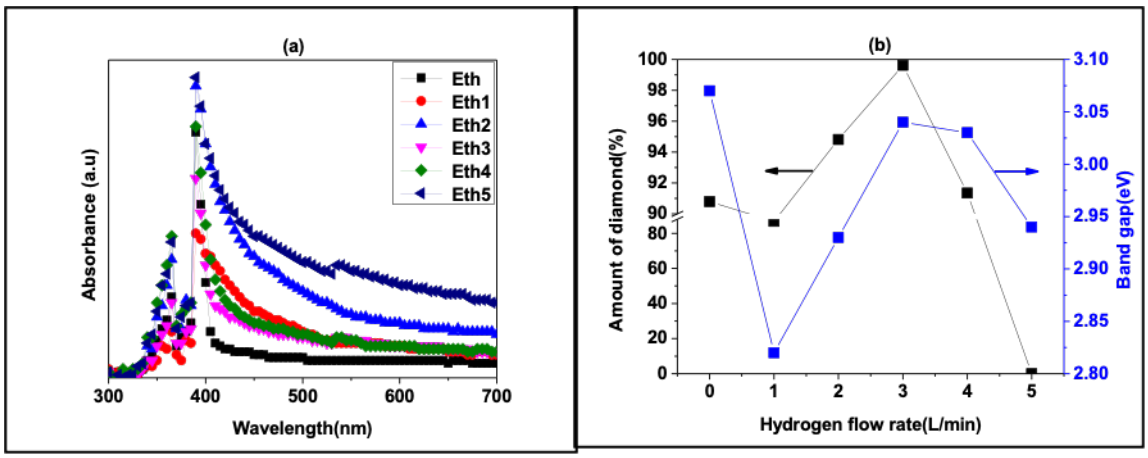

Figure 4. (a) UV-Visible spectrum of NDs at different Hydrogen flow rates, where Eth=constant Argon flow rate= 5L/min. Ethi= Hydrogen flow rate, i= 1-5 L/min (b) variation of I_{Dia}/I_G and band gap of NDs without and with Hydrogen at different flow rates=1-5 L/min.

diamond for different Hydrogen flow rates. To calculate the optical band gap energy from UV Visible absorption spectra, the Tauc relation is used. The reduction in effective band gap with the increase in Hydrogen flow rate (0-2 L/min) is attributed to reduced amount of diamond. The increased sp^2 Carbon content produces defect states within the electronic band gap (mid gap or localized states). Non-diamond phases introduce n to π transition within diamond band gap, shorten the lifetime of excited states and reduce the effective band gap of NDs[33]. Afterward, it starts increasing and obtains the maximum value at the optimum Hydrogen flow rate (3 L/min). Hydrogen efficiently removes the non-diamond phases and results in the increase in band gap. An enhancement in amount of non-diamond phases at higher Hydrogen flow rates (4-5 L/min) decreases the band gap. NDs have a mixture of sp^2 and sp^3 sites in highly disordered grain boundary matrix. The conjugated bonds on the surface of NDs introduced microstrain which create deep and shallow levels within the band gap. An enhancement in π-σ bond mixing is observed due to bond angle distortion. This will result in transitions from sp^2 sites to the antibonding distorted sp3 states.[34] The Nitrogen vacancy defects offer emerging application as quantum computer, fluorescence marker, and nanoscale sensors for electric field, magnetic field, temperature, ion concentration and spin densities.[2,35,36]

Photoluminescence spectroscopy

PL spectra of NDs without and with hydrogen at 3L/min is shown in Figure 5 (a). It exhibits broad PL response from 375-625 nm at an excitation wavelength of 325 nm. The broad PL emission centered at 468 nm was observed from the NDs (without hydrogen). It is related to N_2 defect center[37–40] . It is part of the well-known "cape" spectrum in many yellow diamon[29]. It is attributed to a vibronic transition at the N_3 center in which the electronic excitation is forbidden[41].

With the introduction of hydrogen, the PL peak at 440 nm occurs predominantly due to N_3 defect which naturally exists in type Ia diamond.[38–40] The N_3 center is the most common color-producing defect in diamond, consisting of a vacancy surrounded by three nitrogen atoms on a {111} plane.

Figure 5 (b) shows a variation of PL maximum peak position and I_{Dia}/I_G of NDs without and with hydrogen at 3L/min. A blue shift in peak position is observed with the introduction of hydrogen. PL peaks appeared due to defects or impurities produced in the crystallization process[42] . The blue shift of maximum PL is related to the annihilation of defect or removal of non-diamond phase on the surface. An increase in diamond quality decreases the defect density and shifts the corresponding peaks towards lower wave number[43] . Figure 5 (b) shows the variation of PL intensity and I_{Dia}/I_G of NDs without and with hydrogen at 3L/min. PL intensity and I_{Dia}/I_G exhibits almost opposite behavior. With the increase in diamond quality, a decrease in degeneration sp^2 bonds on the diamond structure is observed[42] . The reduction in the size of NDs reduces the total number of nitrogen-vacancy and contributes to the decrease in PL intensity[44] . As in our case, NDs produced at optimal flow rate has smaller grain size (~1-20 nm) as compared to the sizes (4-32 nm) obtained without hydrogen. Thus one expects lower absorption[1] .

From detail examination, small spikes appear on the continuum contour of PL spectrum at 380 nm, 400 nm, 415 nm, 503 nm, 540 nm, and 612 nm. The different emission peak originates from diamond surface defect, vacancies and impurities (nitrogen, hydrogen, carbon as graphite) attached to the surface[45]

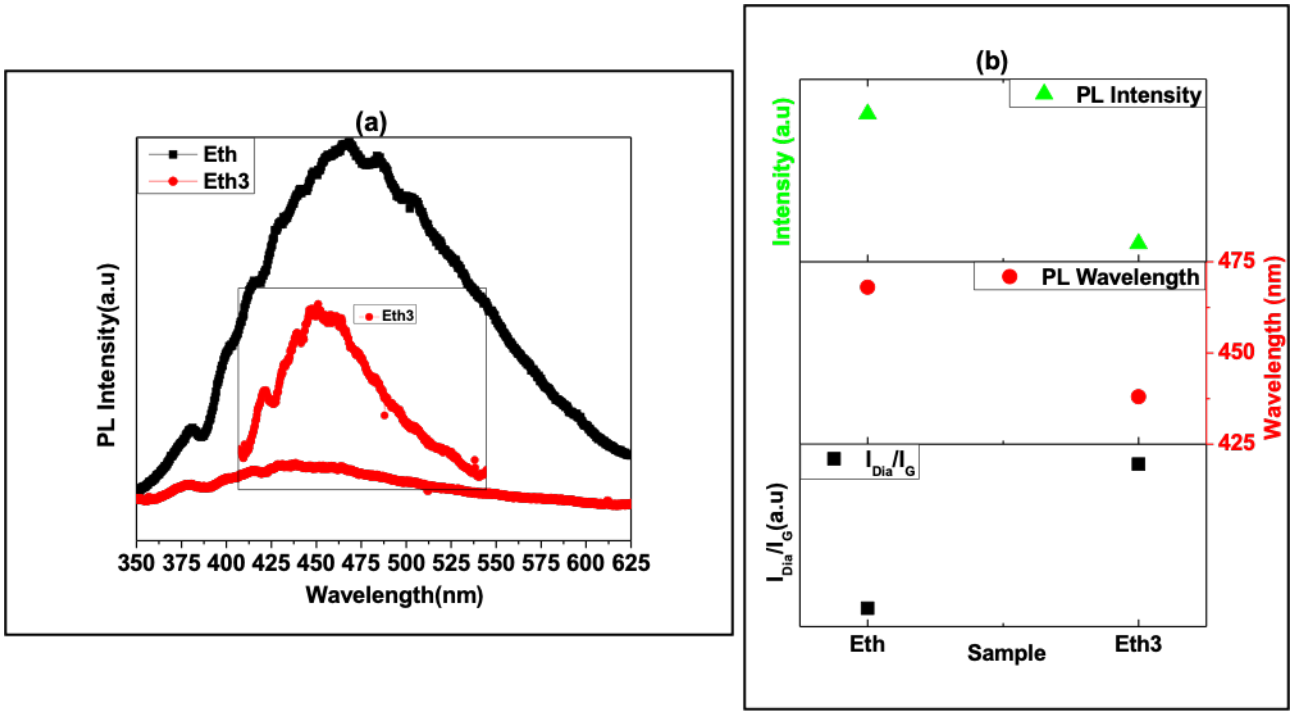

Figure 5. (a) PL spectra of NDs without Hydrogen and with Hydrogen at 3 L/min flow rate. Inset is enlarged image of NDs with Hydrogen at 3 L/min flow rate. (b) Variation of I_{Dia}/I_G with PL peak position and PL intensity of NDs where Eth= constant Argon flow rate= 5L/min. Ethi= Hydrogen flow rate, i= 1-5 L/min.

as confirmed later from FTIR (Figure 6). The small intensity peaks around 380 nm are related to band edge transitions[46]. These PL lines at 413 nm,503 nm and 612 nm are related to N_3, H_3 and NV^- defect[29].

Fourier transform infrared spectroscopy

The FTIR in Figure 6 shows the evolution of surface bonded molecules on NDs without and with Hydrogen at different flow rates. The position and shape of bands strongly depend on the interaction between the surface functional groups of NDs and Hydrogen[2] .

An intense and broadband around (3426-3451 cm^{-1}) is assigned to the O-H vibrations. Intra- and inter-molecular bonds of Hydrogen to the surface of NDs are responsible for this broadening[2,14]. The peak at 2361 cm^{-1} is due to the adsorption vibration of CO2[47]. The band around 3400 cm^{-1} also assigned to N-H vibration[14]. A well-defined absorbance band (1640 cm^{-1}) is ascribed to skeletal vibrations of aromatic groups C=C[2,14]. The peak at 3018 cm^{-1} also corresponds to C=C[48] . The amorphous or disordered sp^2 Carbon acts as catalytic effect. Some of these fragments could be removed from NDs surface in the form of gas phase radicals (C_2, or C_3,) under low temperature. The high energy carbon radicals collide and transform molecular Hydrogen into atomic Hydrogen. The lowest density Hydrogen gains the highest kinetic energy and interacts dominantly with the surface Carbon dangling bond. This ultimately results into the CH adsorption on NDs along with the dissociation of oxygen-related groups and etching of graphitic shell/ non-diamond phase. The Hydrogenation efficiency is dependent on production of atomic Hydrogen in microplasma[2,14] .

Asymmetric CH_3(1362-1366 cm^{-1}), asymmetric CH_2(1427-1436 cm^{-1}), rocking CH (898.6 cm^{-1}) bands confirm the Hydrogenation of NDs surface[2,14] . All the peaks (3006-3012 cm^{-1},1429 cm^{-1},898.6 cm^{-1}) confirm the presence of t-PA [trans-(CH)x] as suggested by our Raman results (Figure 2). Carbonyl, C=O stretching bands (1712.48-1738.51 cm^{-1}) together with the OH stretching bands (3414 cm^{-1}) from the COOH groups indicating the presence of carboxylic acid. Peaks at 1090 cm^{-1} and 1263 cm^{-1} arise from the various stretching mode of carboxylic, ester, ether and alcohol moieties (COC, C-OH)[2,14] . Hydrogenation contributes to the elimination of hydrophilic surface functional groups such as Carbonyl and carboxyl. The disappearance of C-OH is related to depletion of OH group (as confirmed from FTIR). The removal of oxygen-related groups with increasing Hydrogen flow rate is related to high reaction cross section of Hydrogen to oxygen as compared to Carbon or other species (such as Nitrogen). The FTIR spectra of Hydrogenated NDs show

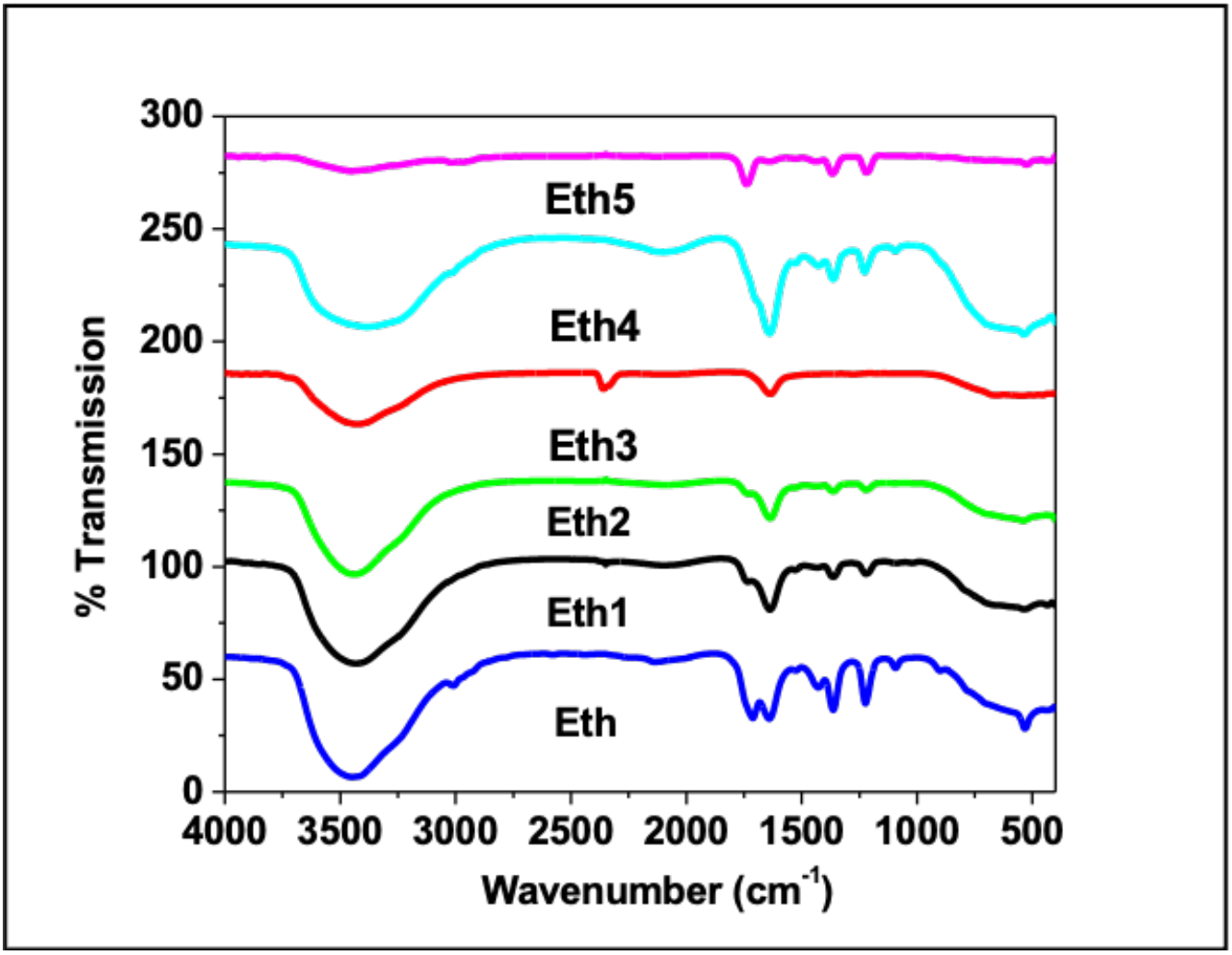

Figure 6. FTIR spectra of NDs without and with Hydrogen at different flow rates=1-5 L/min. where Eth= constant Argon flow rate= 5L/min. Ethi= Hydrogen flow rate, i= 1-5 L/min.

a significant blue shift and weakening of C=C stretching band. Hydrogen etches the non-diamond phases as predicated from literature [12] . The highest graphitic characteristic at high flow rate (4 L/min) is confirmed from I_D/I_G ratio.

CONCLUSIONS

The objective of this work was to analyze the impact of Hydrogen flow rate on NDs synthesis. The 3 L/minis found to be the optimal Hydrogen flow rate for the growth of quality NDs. The smallest size and near stress-free NDs are obtained at this flow rate. The highest amount of Carbon in diamond form also confirmed that the required residence time to satisfy the Hydrogen role (such as quenching, etching, and stabilizing) was finally obtained at flow rate of 3 L/min. Nitrogen-vacancy center along with Nitrogen Hydrogen vacancy complex became active at this optimal flow rate. Nature of nitrogen vacancy complexes can be controlled with the flow rate. These defect centers make diamond a promising material for atomic physicist. The optical transparency of diamond allows long room temperature lifetimes for color centers. NDs offer emerging applications in optoelectronic systems, biomedical nanodevices and nanoscale sensors for electric field, magnetic field & temperature.

CONFLICTS OF INTEREST STATEMENT

The authors have NO affiliations with or involvement in any organization or entity with any financial interest (such as honoraria; educational grants; participation in speakers' bureaus; membership, employment, consultancies, stock ownership, or other equity interest; and expert testimony or patent-licensing arrangements), or non-financial inter-

est (such as personal or professional relationships, affiliations, knowledge or beliefs) in the subject matter or materials discussed in this manuscript.

References

1) Mochalin, V. N.; Shenderova, O.; Ho, D.; Gogotsi, Y. The Properties and Applications of Nanodiamonds. *Nano-Enabled Medical Applications* **2020**, *7*, 313–350.
2) Iqbal, S.; Rafique, M. S.; Zahid, M.; Bashir, S.; Ahmad, M. A.; Ahmad, R. A. Impact of carrier gas flow rate on the synthesis of nanodiamonds via microplasma technique. *Materials Science in Semiconductor Processing* **2018**, *74*, 31–41.
3) Afandi, A.; Howkins, A.; Boyd, I. W.; Jackman, R. B. Nanodiamonds for device applications: An investigation of the properties of boron-doped detonation nanodiamonds. *Scientific Reports* **2018**, *8* (1), 3270–3270.
4) Prabhakar, N.; Rosenholm, J. M. Nanodiamonds for advanced optical bioimaging and beyond. *Current Opinion in Colloid & Interface Science* **2019**, *39*, 220–231.
5) Huang, G.; Ghalei, B.; Isfahani, A. P.; Karahan, H. E.; Terada, D. E.; Qin, D.; Li, C.; Tsujimoto, M.; Yamaguchi, D.; Sugimoto, K.; Igarashi, R.; Chang, B. K.; Li, T.; Shirakawa, M.; Sivaniah, E. Overcoming humidity-induced swelling of graphene oxide-based hydrogen membranes using charge-compensating nanodiamonds. *Nature Energy* **2021**, *6* (12), 1176–1187.
6) Basso, L.; Cazzanelli, M.; Orlandi, M.; Miotello, A. Nanodiamonds: Synthesis and Application in Sensing, Catalysis, and the Possible Connection with Some Processes Occurring in Space. *Applied Sciences* **2020**, *10* (12), 4094–4094.
7) Chauhan, S.; Jain, N.; Nagaich, U. Nanodiamonds with powerful ability for drug delivery and biomedical applications: Recent updates on in vivo study and patents. *Journal of Pharmaceutical Analysis* **2020**, *10* (1), 1–12.
8) Mitev, D. P.; Alsharabasy, A. M.; Morrison, L.; Wittig, S.; Diener, C.; Pandit, A. Plasma & Microwaves as Greener Options for Nanodiamond Purification: Insight Into Cytocompatibility. *Frontiers in Bioengineering and Biotechnology* **2021**, *9*.
9) Park, H. S.; Kim, S. J.; Joh, H. M.; Chung, T. H.; Bae, S. H.; Leem, S. H. Optical and electrical characterization of an atmospheric pressure microplasma jet with a capillary electrode. *Physics of Plasmas* **2010**, *17* (3), 033502–033502.
10) Lin, P. A.; Kumar, A.; Sankaran, R. M. New Insights into Plasma-Assisted Dissociation of Organometallic Vapors for Gas-Phase Synthesis of Metal Nanoparticles. *Plasma Processes and Polymers* **2012**, *9* (11-12), 1184–1193.
11) Du, C.; Liu, Y.; Huang, Y.; Li, Z.; Men, R.; Men, Y.; Tang, J. Qualitation and Quantitation on Microplasma Jet for Bacteria Inactivation. *Scientific Reports* **2016**, *6* (1), 18838–18838.
12) Kumar, A.; Lin, P. A.; Xue, A.; Hao, B.; Yap, Y. K.; Sankaran, R. M. Formation of nanodiamonds at near-ambient conditions via microplasma dissociation of ethanol vapour. *Nature Communications* **2013**, *4* (1).
13) Dychalska, A.; Popielarski, P.; Franków, W.; Fabisiak, K.; Paprocki, K.; Szybowicz, M. Study of CVD diamond layers with amorphous carbon admixture by Raman scattering spectroscopy. *Materials Science-Poland* **2015**, *33* (4), 799–805.
14) Iqbal, S.; Rafique, M. S.; Akhtar, S.; Liaqat, N.; Iqbal, N.; Ahmad, R. A comparative study on finding an effective root for the introduction of hydrogen into microplasma during diamond growth. *Journal of Physics and Chemistry of Solids* **2018**, *122*, 72–86.
15) Lu, Y.; Xu, S. F.; Zhong, X. X.; Ostrikov, K.; Cvelbar, U.; Mariotti, D. Characterization of a DC-driven microplasma between a capillary tube and water surface. *EPL (Europhysics Letters)* **2013**, *102* (1), 15002–15002.
16) Khmelnitskiy, R. Prospects for the synthesis of large single-crystal diamonds. *Physics-Uspekhi* **2015**, *58* (2), 134–149.
17) Shiell, T. B.; Mcculloch, D. G.; Bradby, J. E.; Haberl, B.; Boehler, R.; Mckenzie, D. R. Nanocrystalline hexagonal diamond formed from glassy carbon. *Scientific Reports* **2016**, *6* (1), 37232–37232.
18) Ruan, J.; Yuan, T.; Pang, Y.; Luo, S.; Peng, C.; Yang, J.; Zheng, S. Nitrogen and sulfur dual-doped carbon films as flexible free-standing anodes for Li-ion and Na-ion batteries. *Carbon* **2018**, *126*, 9–16.
19) Ohfuji, H.; Irifune, T.; Litasov, K. D.; Yamashita, T.; Isobe, F.; Afanasiev, V. P.; Pokhilenko, N. P. Natural occurrence of pure nano-polycrystalline diamond from impact crater. *Scientific Reports* **2015**, *5* (1), 14702–14702.
20) Blank, V. D.; Kulnitskiy, B. A.; Nuzhdin, A. A. Lonsdaleite formation in process of reverse phase transition diamond–graphite. *Diamond and Related Materials* **2011**, *20* (10), 1315–1318.
21) Turneaure, S. J.; Sharma, S. M.; Volz, T. J.; Winey, J. M.; Gupta, Y. M. Transformation of shock-compressed graphite to hexagonal diamond in nanoseconds. *Science Advances* **2017**, *3* (10).
22) Shenderova, O. A.; Gruen, D. M. In *Ultrananocrystalline diamond: synthesis, properties and applications*; and others„ Ed.; William Andrew, 2012.
23) Tan, D.; Zhou, S.; Xu, B.; Chen, P.; Shimotsuma, Y.; Miura, K.; Qiu, J. Simple synthesis of ultra-small nanodiamonds with tunable size and photoluminescence. *Carbon* **2013**, *62*, 374–381.
24) Baldan, M. R.; Ramos, S. C.; Almeida, E. C.; Azevedo, A. F.; Ferreira, N. G. Homogeneous micro and nanocrystalline diamond coating on reticulated vitreous carbon treated at different temperatures. *Diamond and Related Materials* **2008**, *17* (7-10), 1110–1115.
25) Wang, W. L.; Polo, M. C.; Sánchez, G.; Cifre, J.; Esteve, J. Internal stress and strain in heavily boron-doped diamond films grown by microwave plasma and hot filament chemical vapor deposition. *Journal of Applied Physics* **1996**, *80* (3), 1846–1850.
26) Stehlik, S.; Varga, M.; Ledinsky, M.; Miliaieva, D.; Kozak, H.; Skakalova, V.; Mangler, C.; Pennycook, T. J.; Meyer, J. C.; Kromka, A.; Rezek, B. High-yield fabrication and properties of 1.4 nm nanodiamonds with narrow size distribution. *Scientific Reports* **2016**, *6* (1), 38419–38419.
27) Zhang, T. F.; Kim, K.-W.; Kim, K. H. Nitrogen-Incorporated Hydrogenated Amorphous Carbon Film Electrodes on Ti Substrates by Hybrid Deposition Technique and Annealing. *Journal of The Electrochemical Society* **2016**, *163* (3), E54–E61.
28) Wang, W.; Hall, M. S.; Moe, K. S.; Tower, J.; Moses, T. M. Latest-Generation CVD-Grown Synthetic Diamonds From Apollo Diamond Inc. *Gems & Gemology* **2007**, *43* (4), 294–312.
29) Breeding, C. M.; Shigley, J. E. The "Type" Classification System of Diamonds and Its Importance in Gemology. *Gems & Gemology* **2009**, *45* (2), 96–111.
30) Meng, Y.-F.; Yan, C.-S.; Lai, J.; Krasnicki, S.; Shu, H.; Yu, T.; Liang, Q.; Mao, H.-K.; Hemley, R. J. Enhanced optical properties of chemical vapor deposited single crystal diamond by low-pressure/high-temperature annealing. *Proceedings of the National Academy of Sciences* **2008**, *105* (46), 17620–17625.
31) Moreno-trejo, M.; Sánchez-domínguez, M. Mesquite Gum as a Novel Reducing and Stabilizing Agent for Modified Tollens Synthesis of Highly Concentrated Ag Nanoparticles. *Materials* **2016**, *9* (10), 817–817.
32) Paul, R.; Das, S. N.; Dalui, S.; Gayen, R. N.; Roy, R. K.; Bhar, R.; Pal, A. K. Synthesis of DLC films with different sp2/sp3 ratios and their hydrophobic behaviour. *Journal of Physics D: Applied Physics* **2008**, *41* (5), 055309–055309.
33) Gupta, S.; Weiner, B. R.; Morell, G. Spectroscopic ellipsometry studies of nanocrystalline carbon thin films deposited by HFCVD. *Diamond and Related Materials* **2001**, *10* (11), 1968–1972.
34) Stuchliková, T. H.; Remes, Z.; Mortet, V.; Taylor, A.; Ashcheulov, P.; Stuchlik, J. Electrical and optical characteristics of boron doped nanocrystalline diamond films. *Vacuum* **2019**, *168*, 108813–108813.
35) Lesik, M.; Plays, T.; Tallaire, A.; Achard, J.; Brinza, O.; William, L.; Chipaux, M.;

Toraille, L.; Debuisschert, T.; Gicquel, A.; Roch, J. F.; Jacques, V. Preferential orientation of NV defects in CVD diamond films grown on (113)-oriented substrates. *Diamond and Related Materials* **2015**, *56*, 47–53.
36) Balasubramanian, G.; Lazariev, A.; Arumugam, S. R.; Duan, D.-W. Nitrogen-Vacancy color center in diamond—emerging nanoscale applications in bioimaging and biosensing. *Current Opinion in Chemical Biology* **2014**, *20*, 69–77.
37) Gaillou, E.; Post, J. E.; Bassim, N. D.; Zaitsev, A. M.; Rose, T.; Fries, M. D.; Stroud, R. M.; Steele, A.; Butler, J. E. Spectroscopic and microscopic characterizations of color lamellae in natural pink diamonds. *Diamond and Related Materials* **2010**, *19* (10), 1207–1220.
38) Shigley, J. E.; Breeding, C. M. Optical Defects in Diamond: A Quick Reference Chart. *Gems & Gemology* **2013**, *49* (2), 107–111.
39) Luo, Y.; Breeding, C. M.; Fluorescence,; By,; Measurement, D.; Characterization,; Challenges, *Gems & Gemology* **2013**, 49–49.
40) Eaton-Magaña, S.; Post, J. E.; Heaney, P. J.; Walters, R. A.; Breeding, C. M.; Butler, J. E. Fluorescence Spectra of Colored Diamonds Using A Rapid, Mobile Spectrometer. *Gems & Gemology* **2007**, *43* (4), 332–351.
41) Zaitsev, A. M. In *Optical properties of diamond: a data handbook*; and others„ Ed.; Springer Science & Business Media, 2013.
42) Baranauskas, V.; Ceragioli, H. J.; Peterlevitz, A. C.; Tosin, M. C.; Durrant, S. F. Effects of argon dilution of an ethanol/hydrogen gas feed on the growth of diamond by hot-filament chemical vapor deposition. *Thin Solid Films* **2000**, *377-378*, 303–308.
43) Salava, J.; Trojánek, F.; Štěpán Stehlík,; Varga, M.; Rezek, B.; Malý, P. Influence of air annealing on the luminescence dynamics of HPHT nanodiamonds. *Diamond and Related Materials* **2016**, *68*, 62–65.
44) Sotoma, S.; Akagi, K.; Hosokawa, S.; Igarashi, R.; Tochio, H.; Harada, Y.; Shirakawa, M. Comprehensive and quantitative analysis for controlling the physical/chemical states and particle properties of nanodiamonds for biological applications. *RSC Advances* **2015**, *5* (18), 13818–13827.
45) Wang, J. Y.; Ko, T. Y.; Sun, K. W. Photoluminescence and raman spectroscopy of single diamond nanoparticle. *2008 2nd IEEE International Nanoelectronics Conference* **2008**, 186–90.
46) Lu, H.-C.; Lin, M.-Y.; Chou, S.-L.; Peng, Y.-C.; Lo, J.-I.; Cheng, B.-M. Identification of Nitrogen Defects in Diamond with Photoluminescence Excited in the 160–240 nm Region. *Analytical Chemistry* **2012**, *84* (21), 9596–9600.
47) Zou, Q.; Wang, M. Z.; Li, Y. G. Analysis of the nanodiamond particle fabricated by detonation. *Journal of Experimental Nanoscience* **2010**, *5* (4), 319–328.
48) Das, R.; Gang, S.; Nath, S. S. Preparation and Antibacterial Activity of Silver Nanoparticles. *Journal of Biomaterials and Nanobiotechnology* **2011**, *02* (04), 472–475.